

Article

Plasma Treatments and Light Extraction from Fluorinated CVD-Grown (400) Single Crystal Diamond Nanopillars

Mariusz Radtke ^{1,*} , Abdallah Slablab ², Sandra Van Vlierberghe ¹ , Chao-Nan Lin ³,
Ying-Jie Lu ³ and Chong-Xin Shan ³

¹ Department of Organic and Macromolecular Chemistry, Ghent University, PBM, CMaC, 9000 Ghent, Belgium; sandra.vanvlierberghe@ugent.be

² Department of Physics, Saarland University, 66123 Saarbrücken, Germany; abdallah.slablab@physik.uni-saarland.de

³ Henan Key Laboratory of Diamond Optoelectronic Materials and Devices, School of Physics and Microelectronics, Zhengzhou University, Zhengzhou 450001, China; cnlin@zzu.edu.cn (C.-N.L.); yjlu@zzu.edu.cn (Y.-J.L.); cxshan@zzu.edu.cn (C.-X.S.)

* Correspondence: mariusz.radtke@ugent.be

Received: 19 April 2020; Accepted: 28 May 2020; Published: 3 June 2020;
Corrected: 12 October 2022



Abstract: We investigate the possibilities to realize light extraction from single crystal diamond (SCD) nanopillars. This was achieved by dedicated 519 nm laser-induced spin-state initiation of negatively charged nitrogen vacancies (NV^-). We focus on the naturally-generated by chemical vapor deposition (CVD) growth of NV^- . Applied diamond was neither implanted with $^{14}N^+$, nor was the CVD synthesized SCD annealed. To investigate the possibility of light extraction by the utilization of NV^- 's bright photoluminescence at room temperature and ambient conditions with the waveguiding effect, we have performed a top-down nanofabrication of SCD by electron beam lithography (EBL) and dry inductively-coupled plasma/reactive ion etching (ICP-RIE) to generate light focusing nanopillars. In addition, we have fluorinated the diamond's surface by dedicated 0 V SF_6 ICP plasma. Light extraction and spin manipulations were performed with photoluminescence (PL) spectroscopy and optically detected magnetic resonance (ODMR) at room temperature. We have observed a remarkable effect based on the selective 0 V SF_6 plasma etching and surprisingly, in contrast to literature findings, deactivation of NV^- centers. We discuss the possible deactivation mechanism in detail.

Keywords: single crystal diamond; nitrogen vacancies; nanofabrication

1. Introduction

Diamond is the hardest material in Mohs scale that attracts attention spanning from antipodal fields of industrial abrasives to even quantum information [1]. In theory, diamond is composed only of isotopic mixture of sp^3 carbon atoms (^{12}C and ^{13}C), which are ideally aligned in supercells comprised of fused chair conformed cyclohexane rings [2]. However, this idealized imagination of diamond is not complete, as in reality within the supercell not every carbon atom contains saturated bonds, mostly due to the impurities and crystallographic imperfections incorporated into lattice during the growth [3]. The most common impurity is nitrogen (^{14}N), which is vastly present in synthetic diamond, giving it a remarkable yellow appearance [4]. The nitrogen content among other impurities is the basis for its classification ranging from Type 1b to optical and electronic grade. The most common synthetic methods of diamond growth are high pressure high temperature (HPHT) for Types 1a and 1b and chemical vapor deposition (CVD) for Type 2b and electronic grade. As chemical vapor deposition

occurs at elevated temperatures reaching up to 1000 °C and high vacuum reaching several mTorr, the deposited layers are annealed at those conditions [5]. As nitrogen being the main impurity within the diamond supercell in its sp^3 is only able to utilize 3 covalent bonds and due to the fact that carbon (sp^3) can have 4 bonds, the missing gap after incorporation of nitrogen into supercell results in so-called nitrogen vacancy, NV^- [6]. This vacancy has remarkable properties. It behaves like an artificial atom, has a well-defined electronic structure that can be simulated by sophisticated methods of density functional theory (DFT) and most importantly from the quantum sensing perspective—it has an electron spin ($S = 1$) [7]. Density functional theory computational studies combined with experimental work were also undertaken for the approach of elucidating magnetic properties of negatively charged nitrogen vacancies within nanodiamonds as a function of surface termination (hydrogen and oxygen terminated) [8]. The computational work focusing exclusively on fluorine termination of single crystal bulk diamond and its influence on optical properties of negatively charged nitrogen vacancies is still relatively spare. In the negatively charged nitrogen vacancy, the presence of electron spin causes its intrinsic angular momentum to couple to a laser at resonance frequency, causing an excitation and following relaxation resulting in bright photoluminescence already at room temperature. A nitrogen vacancy comes in many different forms, whereby the negatively charged nitrogen vacancy draws most of the attention in quantum-related research field. The reason for that arises from the fact that NV^- has 6 electrons in its structure contributing to the electron spin of $S = 1$ [9]. This electron spin can be optically excited and the resulting fluorescence at room temperature is bright enough to be easily detected by a charge coupled device (CCD) of a standard confocal microscopy. Due to the presence of electron spin, the negatively charged nitrogen vacancy can also couple to the external magnetic field, which influences its fluorescence upon appropriate laser excitation in form of Zeeman effect. This allows the use of diamond in magnetometry, metrology and also quantum computing [10]. All of that is possible as diamond is a material with negligible optical absorption in the region above 220 nm up to even 1000 μm due to its band gap of approximate 5.5 eV (with the exception of a weak absorption line at 5 μm due to the lattice absorption resulting in transformation of photons into phonons) [11].

The enhancement of photoluminescence count-rate arising from NV^- relaxation can be achieved with waveguiding effect. The easiest approach to do so is nanofabrication [12]. Diamond is nevertheless an insulator, which makes it a challenging material to perform standard lithography by means of electron beam (EBL) and use of reactive ions in plasma to etch it (ICP/RIE), mostly due to the capacitive charging effects deflecting the beam and blurring the written pattern, which also suffers from the lack of adhesion to the most common lithographic resins. These nanofabrication issues can be resolved by sophisticated use of decharging layers and dedicated plasma technology [12]. Other method to increase the photoluminescence count-rate and stability of NV^- in diamond is the use of dedicated surface termination. The most common cause of drop in photoluminescence signal from NV^- is loss of one electron from its intrinsic electronic structure due to the photoelectric effect induced by the incident laser. The ejection of an electron from the valence to conduction band causes the transition of NV^- into the optically dormant NV^0 state with 5 electrons that cannot be optically read-out. As it was already described by others, this loss can be controlled by shifting the Fermi level between the valence and conduction band in diamond being already separated by 5.5 eV energy gap [13]. The electron donating counterparts (hydrogen or methyl) cause the Fermi level to rise and therefore facilitate electron ejection upon laser excitation (see Figure 1). The use of electron-withdrawing groups like carboxyl, carbonyl or halogen groups has an opposite effect. The Fermi level drops, while the effective transition dipole moment of diamond changes its orientation and electron ejection is no more energetically unfavorable [14]. This has an advantage for the nitrogen vacancy to retain its stability upon constant laser excitation. The most promising candidate for this process is fluorine termination.

The currently investigated methods are wet chemical and plasma procedures [15]. Chemical fluorination does not cause surface roughening, but is on the other hand lengthy in time due to the chemical inertness and difficulties to ensure activation of C–H bond [16]. Plasma methodology is on the contrary very quick and convenient, yet can nevertheless cause surface roughening that leads to

photoluminescence signal loss. In the present study, we have developed a type of 0 V SF₆ plasma and investigated its effect on CVD grown diamond with nitrogen vacancies generated by in-situ annealing during the growth process. Surprisingly, we have observed a selective deactivation of the naturally generated NV⁻ caused by fluorination.

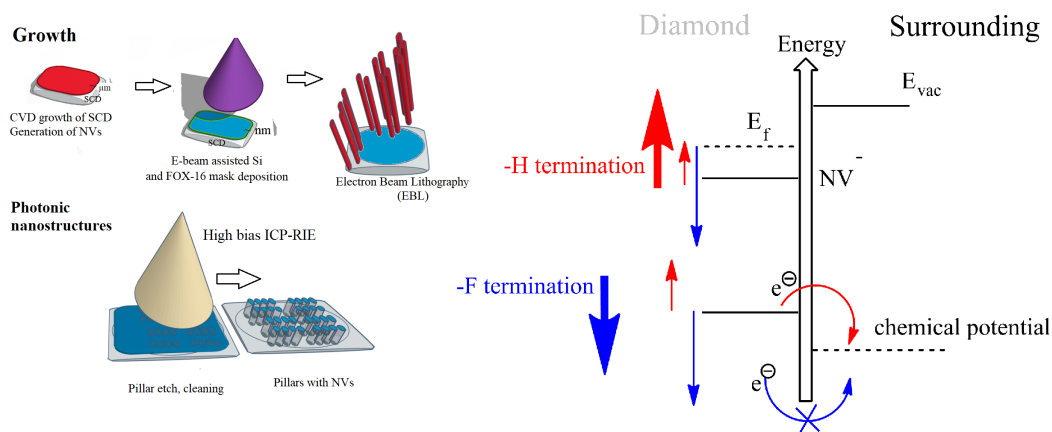


Figure 1. Left: generation of photonic nanostructures in chemical vapor deposition (CVD)-grown single crystal diamond containing naturally grown-in, negatively charged nitrogen vacancies. Right: Effects of surface termination on the electron loss from a negatively charged nitrogen vacancy on example hydrogen and fluorine termination. In this study plasma fluorination with heavy SF₆ ions was applied.

2. Results and Discussion

2.1. Photonic Properties of as-Grown Diamond and after Successful Nanofabrication

Naturally grown-in nitrogen vacancies have shown a remarkable stability during irradiation. It has been observed by others that negatively charged nitrogen vacancies usually change their charge state from -1 to neutral and sometimes even $+1$ upon prolonged laser exposure [17]. This is caused by ejection of electrons from the valence to the conduction band. In case of naturally grown nitrogen vacancies, we have observed the prolonged stability of the charge state, allowing for the multiple accumulation of photoluminescence maps and optically detected magnetic resonance (ODMR) signals with and without applied magnetic field Figure 2. We note the fact that single application of the magnetic field induced a degeneration of $m_s = \pm 1$ state and a drop of the photoluminescence signal at the 2.87 GHz transition frequency, which usually requires multiple scans in order to obtain an improved signal to noise ratio. As the ground state of a nitrogen vacancy consists of a pair of ground and excited triplet and singlet states, the triplet ground state is made up of $m_s = \pm 1$ and lower in energy $m_s = 0$ Figure 3. As the \pm ground state lies higher in energy, it is easier to excite it with e.g., a green 519 nm laser, which brings the nitrogen vacancy to its excited triplet state. There are three possibilities for a relaxation here. First two possibilities occurs simultaneously into 637 nm i.e., so-called purely electronic transition, zero phonon line (ZPL) to the $m_s = \pm 1$ and less energetically favored $m_s = 0$ state [18]. At room temperature these two transitions are seen as one ZPL, while at cryogenic temperatures, it is possible to observe two distinct lines [18]. Indeed these transitions occur within one triplet system, as they are symmetrically allowed. $m_s = \pm 1$ is therefore described as “bright state”, which contributes most strongly to the observed PL signal. There is also a possibility of an other transition caused by intersystem crossing from the excited triplet state to the singlet state. As this transition is “forbidden” by symmetry rules, it occurs at significantly slower rates compared to the triplet-triplet transitions and the return to the $m_s = 0$ state is called a “dark” transition while m_s is a “dark state” [19]. By sweeping the magnetic field around the photonic nanostructures, we observed a typical resonance at 2.87 GHz for negatively charged nitrogen vacancies. This resonance is typical for

the $m_s = \pm 1 \rightarrow m_s = 0$ cycling transition. We note that by application of the external magnetic field, we observed a noisy splitting of the sharp singlet to a characteristic set of 4 doublets, indicating the $m_s = 0 \rightarrow m_s = 1$ and $m_s = 0 \rightarrow m_s = -1$ transitions in all four possible crystallographic directions of NV^-s [20]. In addition, we have performed an analysis of the ODMR signals between the pillars, which is shown in the inset d of the Figure 2. The theoretical resolution of the microscope objective of 0.8 numerical aperture and due to the use of 519 nm laser is 324 nm. We note that due to the area of interest, which was chosen as a double of the theoretical resolution, this signal might be contaminated by the presence of nitrogen vacancies in the neighboring pillars, as it the ROI is larger than the pillar itself. It can be clearly seen in poor fit of the ODMR signal, which even after mixing Gaussian and Lorentzian contributions did not exceed R^2 value of 0.4 (inset d, middle). We saw a remarkable drop in the ODMR resolution, nevertheless the signature of the nitrogen vacancies could be still recognized. In order to eliminate the possibility of ODMR signal contamination, we have performed an additional scan in the etched area, which turned out not to show the characteristic for the negatively charged nitrogen vacancies dip at 2.87 GHz. It might be an indication for the fact that the naturally generated nitrogen vacancies lay close to the surface, which was etched away during the dry etching process in nanofabrication.

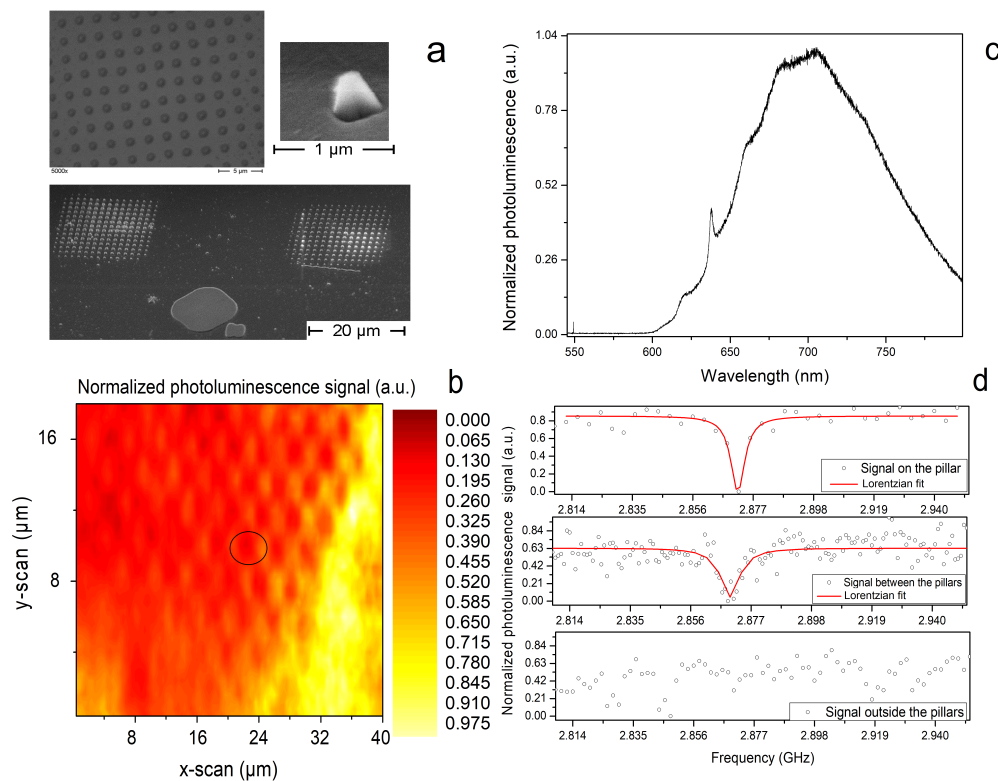


Figure 2. Generation of diamond nanopillars on 2.3 cm thick CVD-grown diamond plate (a) and their photoluminescence mapping (b). The circle indicates the area of interest, which was calculated to be 648 nm in size. Inset (c) represents photoluminescence spectrum with clear zero phonon line (ZPL) emerging from the presence of negatively charged nitrogen vacancy and Raman diamond line at 551 nm, which was investigated further by means of Raman spectroscopy in further sections. Inset (d) shows optically detected magnetic resonance investigation with characteristic 2.87 GHz transition emerging from the degeneration of the $m_s = \pm 1$ state within nitrogen vacancy in pillars (top), between the pillars (middle) and outside the pillars (bottom). The actual area of interest for the optically detected magnetic resonance (ODMR) measurements was found to be 7 MHz.

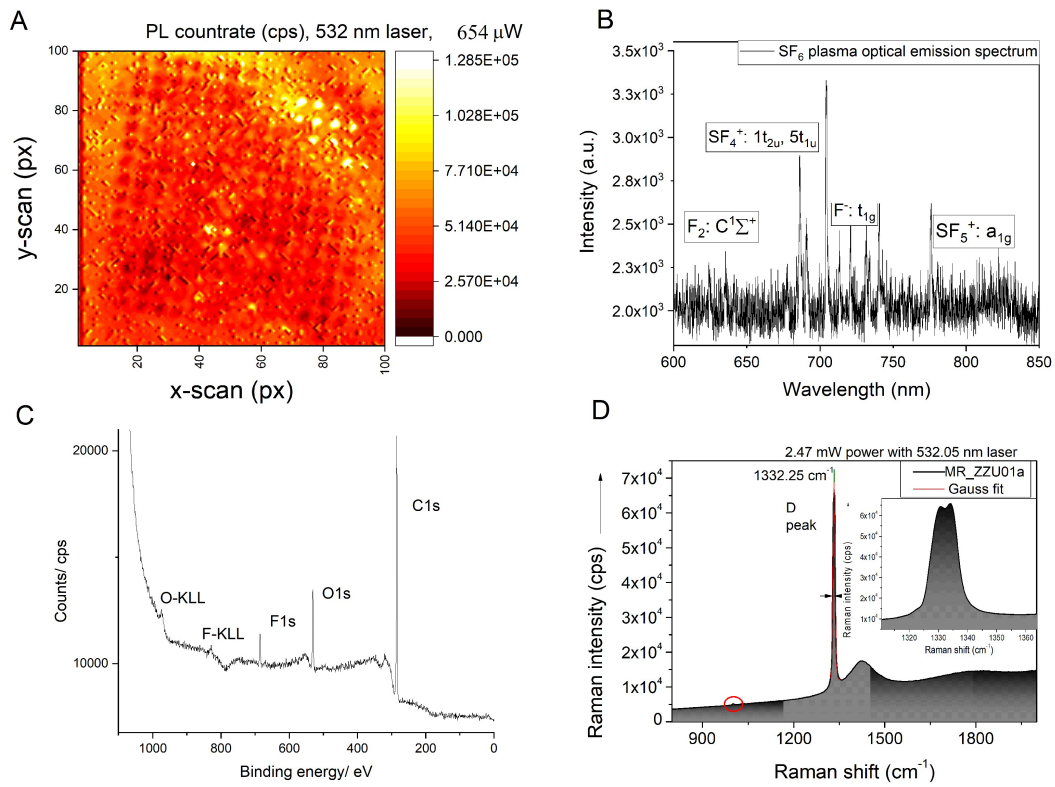


Figure 3. (A) Photoluminescence scan of nanopillars etched into diamond after 0 V bias plasma fluorination. The pillars were partially covered with single crystal quartz plate in order to shield them from the influence of plasma. Such an approach allows quantification of the fluorine termination on negatively charged nitrogen vacancies. An effect of photoluminescence quenching is clearly visible. (B) Optical emission spectrum of 0 V bias SF_6 used to fluorinate the diamond with respective transitions. (C) XPS spectrum of the plasma-fluorinated CVD-grown diamond. (D) Dedicated Raman spectrum showing splitting of D-band due to the growth-induced stress, which serves as a proof for lack of underetching.

2.2. 0 V SF_6 Plasma-Aided Fluorination of Single Crystal Diamond

Inspired by the recent research performed on diamond surface modifications, we have attempted to fluorinate the surface of diamond to increase the stability of NV^- upon laser irradiation [21]. The electron withdrawing character of halogenide, especially the fluorine, decreases the Fermi level of the nitrogen vacancy closer to its vacuum level, making loss of electron less plausible. Surprisingly, we have observed a switching of NV^- to NV^0 upon surface termination. The effective surface termination was proven by X-ray photoelectron spectroscopy (XPS) and the presence of F1s and F KLL lines in the survey spectrum. Due to the insulating character of diamond and therefore the surface charging effects, the exact position of F1s and F KLL should not be taken as an absolute value, as it depends on the level of surface polarization [22]:

$$\left[\frac{-\hbar}{2m_n} \frac{d^2}{dz^2} + V_z \right] \psi_i(z) = \epsilon_i \psi_i(z) \quad (1)$$

$$\frac{d^2\Phi}{dz^2} = -\frac{\rho(z)}{\epsilon} = -\frac{1}{\epsilon} 2q \left[\sum_{mn} \sum_i f(\epsilon) \psi_i^*(z) \right] + eN_0 = \frac{2q}{\epsilon} \sum_i N_i \psi_i^2(z) + eN_0 \quad (2)$$

Here z is the term used to describe charge distance from the surface, $\psi_i(z)$ is the i -th hole sub-band state wave function of eigenenergy ϵ_i . $\Phi(z)$ describes the electrostatic potential, q is the charge, $\rho(z)$ stands for the charge density, which is inversely proportional to the eigenenergy ϵ_i .

2.3. Effect of Fluorination on Charge Loss in Negatively-Charged Nitrogen Vacancy

Fluorination lowers the Fermi level of the nitrogen, making electron loss from successfully generated negatively charged nitrogen vacancy NV^- thermodynamically favorable. According to Equation (2), as the Fermi level is lowered in energy, the charge density drops. We attribute this phenomenon to electron transfer from NV^- to $^{14}N^+$. Many existing reports include possibilities of NV^- activation by respective fluorine termination of the surface by means of plasma or wet chemical covalent (fluoride) and non-covalent (fluorine) termination [15,16,23]. In contrast with these findings, we have observed selective deactivation of those color centers. This was performed by selective coverage of photonic structures by a quartz plate, of which most of the nanopillars were exposed to seemingly anisotropic SF_6 0 V plasma. Here, we present an optical emission spectrum of this plasma showing the respective fluorine transitions being the source of effective surface termination. The respective transitions were assigned in Figure 3, which shows a possible mechanism of SF_6 decomposition. The deactivation of the NV^- centers was irreversible.

2.4. Selective Fluorination and Thermodynamical Instability

In order to exclude the possibility of underetching and refer only to the fluorination induced deactivation of negatively charged nitrogen vacancies, we have performed dedicated Raman measurements on diamond prior and after the plasma treatment. We have observed no change in full width at half maximum in Raman D-band shown in the Figure 3. In addition to that we have preserved the D-band splitting occurring due to the presence of large stress within the outer surface. This observation was aided by root mean square roughness measurements by means of atomic force microscopy, which has shown no change. The actual influence was observed within photoluminescence count-rate, which dropped by an order of magnitude after exposure to 0 V bias SF_6 plasma. We refer the fact of selective deactivation of negatively charged nitrogen vacancies to their thermodynamical instability [24]. The nitrogen vacancies were not annealed and therefore even slight changes in the crystallographic surrounding induced by the bombardment with heavy ions like SF_5^+ cause a change to energetically more favorable neutral state. This assumption is well supported by the fact that large strain present in the diamond after CVD growth observed in Raman spectrum (Figure 3D). Similar procedures with fluoromethane plasma on diamond with $^{14}N^+$ implanted by ion implantation techniques followed by high temperature high vacuum annealing has provided promising results, as well as the wet chemical fluorination [23]. In contrast, in this study the fluorination induced charge state switching within naturally generated nitrogen vacancy was found to be irreversible. We attribute this effect to the presence of unreacted atomic nitrogen in the diamond as well as strain inducing physical etching with heavy SF_6 plasma.

3. Materials and Methods

3.1. CVD Diamond Growth

Single crystal diamond was grown by chemical vapor deposition according to the procedure published earlier [25]. The presence of single crystal diamond was confirmed by the X-ray diffraction (XRD) measurement, which resulted with a distinctive peak at 119.8° , which corresponds to (400) orientation [26]. An additional identification of the diamond was performed with vibrational mode Raman spectrometer employing 532.05 nm laser wavelength and 2.25 mW power (Cobolt High Performance lasers, Huebner photonics) and Kaiser optical systems spectrometer (RamanRXN Systems Raman microprobe) equipped with Leica DM 2500P microscope (with Leica Germany 50 × objective of 0.5 numerical aperture). The acquisition time of Raman focused sample was kept at 60 seconds each.

3.2. Nanofabrication

We refer the reader to earlier studies on the nanofabrication published earlier [12]. In brief: we employed a cold-cathode scanning electron microscope (SEM) (Hitachi S4500), equipped with RAITH Elphy software to perform electron beam-lithography (EBL). Immediately after the growth and acid cleaning of diamond, 25 nm thick polycrystalline silicon was evaporated on the surface as adhesive layer and a negative tone resist, FOX16 was spin-coated. The mask structures were written by electron beam lithography. The imaging was performed with Hitachi S800 scanning electron microscope and JEOL JSM-7000 F. The written structures were further etched-in with highly anisotropic pure oxygen RIE/ICP plasma preceded by a short SF₆ pulse. After removing mask and adhesive layer by wet-chemical etching methods (HF-based buffered oxide etchant and followed by immediate 3M KOH bath) as well as acid cleaning (1:1:1 HNO₃, H₂SO₄, HClO₄).

3.3. Photoluminescence Spectroscopy on Naturally Grown-In Nitrogen Vacancies

A custom-built confocal microscope of 0.8 numerical aperture (NA) was used to excite and characterize negatively charged nitrogen vacancies in single crystal diamond. The confocal filtering was facilitated by a single mode fiber and the laser of choice was a continuous diode-pumped solid-state laser (DPSS) with a wavelength of 519 nm. The photoluminescence signal was detected through the application of a 650 nm longpass-filter and Eselitas SPCM-AQRH-14 photon counters. The spin manipulations were performed with a microwave source (Stanford Research Systems, SG 384) and Mini Circuits amplifier, ZHL -42W+. The microwaves were delivered by 20 μm thick gold wire. The optically detected magnetic resonance was acquired in frequency range (GHz): 2.700 to 3.100, stepsize (MHz) 1.0 and was averaged over 10 signals."

4. Conclusions

In conclusion, we have developed a nanostructured photon emitter system based on naturally grown-in and stable nitrogen vacancies within single crystal diamond. We have successfully manipulated the spin of these naturally occurring negatively charged nitrogen vacancies with optically detected magnetometric techniques. These manipulations serve as a proof of concept for distinguishing other color centers present in the SCD. A broad distribution of this sample along the surface was correlated with measurements of NV⁻ density. In addition we have observed that these color centers can be actively switched off by soft fluorination with 0 V-biased fluorine plasma. The possibility of underetching was excluded by observation of D-band splitting in Raman spectrum. As it was already discussed by Strobel et al., we also base the further discussion on the surface p-doping concept [27]. As the fluorinated species tend to have high electronic activity (EA), they are highly prone to generate electron-hole pairs with in solid state systems (ref), which enhances the conductivity and makes diamond not a fully insulating material anymore. As the conductivity is described by the electron transfer from the lower electron affinity (diamond, which has also much lower ionization potential) to the surface of higher electron activity (fluorinated diamond). Electron transfer causes creation an electron-hole pair and resulting from that p-conductivity. Calculations performed by others have shown that fluorination of other carbon allotropes, in this case fullerenes has caused lowering of the activation energy for electron transfer (in case of C₆₀F₃₆ it was reported to increase the electron affinity by 0.3 eV) and resulted in charge transfer as a repercussion [28]. In case of diamond and nitrogen vacancies, in close vicinity to the diamond surface, the resulted p-conductivity upon fluorination may cause a similar effect. As the charge-transfer between nitrogen vacancy and fluorinated diamond surface will be more prone to occur, the lose of an electron is possible. The transfer of nitrogen vacancy at its negative oxidation state to the neutral oxidation state is the main cause for optical inactivity. This effect appears to be even more severe once the diamond surface is fluorinated. It speaks well for the strong electron withdrawing effect of the halogenide attached to the surface (as proven by XPS) and instability upon stress relief induced by physical etching with heavy sulfur ions within the ICP-RIE

chamber. Interestingly, we have observed no signature of a negatively charged silicon vacancy, neither we witnessed any spectroscopic signature of other impurities present in diamond. We refer this effect to the dedicated green laser excitation wavelength used in this studies. The off-resonant excitation of the silicon vacancy was mostly performed with help of 730 nm red laser [29,30]. We also note that the possible presence of negatively charged silicon vacancy (ZPL at 737 nm) might be blurred within the phonon side-band of the nitrogen vacancy, as the experiments in this paper were performed at room temperature. The neutral silicon vacancy with zero phonon line occurring at 946 nm lies outside of our detection limit [31]. An additional factor is the brightness of the negatively charged nitrogen vacancy, which is the main cause for the signal of silicon vacancy to disappear under the phonon side band of NV^- .

Author Contributions: M.R. designed the experiments, provided the ground idea, performed the measurements and conducted all presented experimental work unless otherwise stated, analyzed them and wrote the manuscript. A.S. helped with the ODMR measurements and explanation of the photonic data. S.V.V. provided insightful discussions and supervised the language editing. C.-N.L. and Y.-J.L. grew the single crystal diamond. C.-X.S. served as supervisor of the conducted studies and cordially provided a possibility of mutual work at international scale. All authors have read and agreed to the published version of the manuscript.

Funding: This research received no external funding.

Acknowledgments: We acknowledge Rene Hensel (INM, Germany) for granting access to the ICP-RIE reactor. We note that the nanofabrication method applied in this study is filed for a patent, application number: EP19198772.6.

Conflicts of Interest: The authors declare no conflict of interest.

References

1. Bernardi, E.; Nelz, R.; Sonusen, S.; Neu, E. Nanoscale Sensing Using Point Defects in Single-Crystal Diamond: Recent Progress on Nitrogen Vacancy Center-Based Sensors. *Crystals* **2017**, *7*, 124. [[CrossRef](#)]
2. Chou, J.P.; Bodrog, Z.; Gali, A. First-Principles Study of Charge Diffusion between Proximate Solid-State Qubits and Its Implications on Sensor Applications. *Phys. Rev. Lett.* **2018**, *120*, 136401. [[CrossRef](#)]
3. Barnard, A.S. Diamond standard in diagnostics: nanodiamond biolabels make their mark. *Analyst* **2009**, *134*, 1751–1764. [[CrossRef](#)] [[PubMed](#)]
4. Chakraborty, T.; Lehmann, F.; Zhang, J.; Borgsdorf, S.; Woehrl, N.; Remfort, R.; Buck, V.; Koehler, U.; Suter, D. CVD growth of ultrapure diamond, generation of NV centers by ion implantation, and their spectroscopic characterization for quantum technological applications. *Phys. Rev. Mater.* **2019**, *3*, 065205. [[CrossRef](#)]
5. Osterkamp, C.; Mangold, M.; Lang, J.; Balasubramanian, P.; Teraji, T.; Naydenov, B.; Jelezko, F. Engineering preferentially-aligned nitrogen-vacancy centre ensembles in CVD grown diamond. *Sci. Rep.* **2019**, *9*, 1–7. [[CrossRef](#)] [[PubMed](#)]
6. Hilser, F.; Burkard, G. All-optical control of the spin state in the NV^- center in diamond. *Phys. Rev. B* **2012**, *86*, 125204. [[CrossRef](#)]
7. Fuchs, G.D.; Dobrovitski, V.V.; Hanson, R.; Batra, A.; Weis, C.D.; Schenkel, T.; Awschalom, D.D. Excited-State Spectroscopy Using Single Spin Manipulation in Diamond. *Phys. Rev. Lett.* **2008**, *101*, 117601. [[CrossRef](#)]
8. Kratochvilova, I.; Sebera, J.; Ashcheulov, P.; Golan, M.; Ledvina, M.; Micova, J.; Mravec, F.; Kovalenko, A.; Zverev, D.; Yavkin, B.; et al. Magnetical and Optical Properties of Nanodiamonds Can Be Tuned by Particles Surface Chemistry: Theoretical and Experimental Study. *J. Phys. Chem. C* **2014**, *118*, 25245–25252. [[CrossRef](#)]
9. Gali, A. Ab initio theory of the nitrogen-vacancy center in diamond. *Nanophotonics* **2019**, *8*, 1907–1943. [[CrossRef](#)]
10. Radtke, M.; Bernardi, E.; Slablab, A.; Nelz, R.; Neu, E. Nanoscale sensing based on nitrogen vacancy centers in single crystal diamond and nanodiamonds: Achievements and challenges. *Nano Futures* **2019**, *3*, 042004. [[CrossRef](#)]
11. Mildren, R.P. Intrinsic Optical Properties of Diamond. In *Optical Engineering of Diamond*; Mildren, R.P., Rabeau, J.R., Eds.; Wiley-VCH Verlag GmbH & Co. KGaA: Weinheim, Germany, 2013; pp. 1–34.
12. Radtke, M.; Nelz, R.; Slablab, A.; Neu, E. Reliable Nanofabrication of Single-Crystal Diamond Photonic Nanostructures for Nanoscale Sensing. *Micromachines* **2019**, *10*, 718. [[CrossRef](#)] [[PubMed](#)]

13. Grotz, B.; Hauf, M.V.; Dankerl, M.; Naydenov, B.; Pezzagna, S.; Meijer, J.; Jelezko, F.; Wrachtrup, J.; Stutzmann, M.; Reinhard, F.; et al. Charge state manipulation of qubits in diamond. *Nat. Commun.* **2012**, *3*, 1–6. [[CrossRef](#)] [[PubMed](#)]
14. Li, F.; Zhang, J.; Wang, X.; Zhang, M.; Wang, H. Barrier Heights of Au on Diamond with Different Terminations Determined by X-ray Photoelectron Spectroscopy. *Coatings* **2017**, *7*, 88.
15. Hu, W.; Li, Z.; Yang, J. Surface and size effects on the charge state of NV center in nanodiamonds. *Comput. Theor. Chem.* **2013**, *1021*, 49–53. [[CrossRef](#)]
16. Cui, S.; Hu, E.L. Increased negatively charged nitrogen-vacancy centers in fluorinated diamond. *Appl. Phys. Lett.* **2013**, *103*, 051603. [[CrossRef](#)]
17. Bourgeois, E.; Jarmola, A.; Siyushev, P.; Gulka, M.; Hruby, J.; Jelezko, F.; Budker, D.; Nesladek, M. Photoelectric detection of electron spin resonance of nitrogen-vacancy centres in diamond. *Nat. Commun.* **2015**, *6*, 1–8. [[CrossRef](#)]
18. Su, Z.; Ren, Z.; Bao, Y.; Lao, X.; Zhang, J.; Zhang, J.; Zhu, D.; Lu, Y.; Hao, Y.; Xu, S. Luminescence landscapes of nitrogen-vacancy centers in diamond: quasi-localized vibrational resonances and selective coupling. *J. Mater. Chem. C* **2019**, *7*, 8086–8091. [[CrossRef](#)]
19. Udvarhelyi, P.; Shkolnikov, V.O.; Gali, A.; Burkard, G.; Pályi, A. Spin-strain interaction in nitrogen-vacancy centers in diamond. *Phys. Rev. B* **2018**, *98*, 075201. [[CrossRef](#)]
20. Braukmann, D.; Glaser, E.R.; Kennedy, T.A.; Bayer, M.; Debus, J. Circularly polarized zero-phonon transitions of vacancies in diamond at high magnetic fields. *Phys. Rev. B* **2018**, *97*, 195448. [[CrossRef](#)]
21. Leech, P.W.; Reeves, G.K.; Holland, A. Reactive ion etching of diamond in CF₄, O₂, O₂ and Ar-based mixtures. *J. Mater. Sci.* **2001**, *36*, 3453–3459. [[CrossRef](#)]
22. Cazaux, J. Mechanisms of charging in electron spectroscopy. *J. Electron Spectrosc. Relat. Phenom.* **1999**, *105*, 155–185. [[CrossRef](#)]
23. Nagl, A.; Hemelaar, S.R.; Schirhagl, R. Improving surface and defect center chemistry of fluorescent nanodiamonds for imaging purposes a review. *Anal. Bioanal. Chem.* **2015**, *407*, 7521–7536. [[CrossRef](#)] [[PubMed](#)]
24. Drumm, D.W.; Per, M.C.; Russo, S.P.; Hollenberg, L.C.L. Thermodynamic stability of neutral Xe defects in diamond. *Phys. Rev. B* **2010**, *82*, 054102. [[CrossRef](#)]
25. Chen, Y.C.; Lu, Y.J.; Lin, C.N.; Tian, Y.Z.; Gao, C.J.; Dong, L.; Shan, C.X. Self-powered diamond Ga₂O₃ photodetectors for solar blind imaging. *J. Mater. Chem. C* **2018**, *6*, 5727–5732. [[CrossRef](#)]
26. Zhuo, R.; Wu, D.; Wang, Y.; Wu, E.; Jia, C.; Shi, Z.; Xu, T.; Tian, Y.; Li, X. A self-powered solar blind photodetector based on a MoS₂ Ga₂O₃ heterojunction. *J. Mater. Chem. C* **2018**, *6*, 10982–10986. [[CrossRef](#)]
27. Strobel, P.; Riedel, M.; Ristein, J.; Ley, L.; Boltalina, O. Surface transfer doping of diamond by fullerene. *Diam. Relat. Mater.* **2005**, *14*, 451–458. [[CrossRef](#)]
28. Ouyang, T.; Loh, K.P.; Qi, D.; Wee, A.T.S.; Nesladek, M. Chemical Bonding of Fullerene and Fluorinated Fullerene on Bare and Hydrogenated Diamond. *ChemPhysChem* **2008**, *9*, 1286–1293. [[CrossRef](#)]
29. Nagy, R.; Niethammer, M.; Widmann, M.; Chen, Y.C.; Udvarhelyi, P.; Bonato, C.; Hassan, J.U.; Karhu, R.; Ivanov, I.G.; Son, N.T.; et al. High-fidelity spin and optical control of single silicon-vacancy centres in silicon carbide. *Nat. Commun.* **2019**, *10*, 1954. [[CrossRef](#)]
30. Lang, J.; Haessler, S.; Fuhrmann, J.; Waltrich, R.; Laddha, S.; Scharpf, J.; Kubanek, A.; Naydenov, B.; Jelezko, F. Long optical coherence times of shallow-implanted, negatively charged silicon vacancy centers in diamond. *Appl. Phys. Lett.* **2020**, *116*, 064001. [[CrossRef](#)]
31. Green, B.L.; Mottishaw, S.; Breeze, B.G.; Edmonds, A.M.; D’Haenens-Johansson, U.F.S.; Doherty, M.W.; Williams, S.D.; Twitchen, D.J.; Newton, M.E. Neutral Silicon-Vacancy Center in Diamond: Spin Polarization and Lifetimes. *Phys. Rev. Lett.* **2017**, *119*, 096402. [[CrossRef](#)]

